Title

Defining Nafion Ionomer Roles for Enhancing Alkaline Oxygen Evolution Electrocatalysis

Journal

ACS Catalysis, 8(12)

ISSN

2155-5435

Authors

Li, Guang-Fu
Yang, Donglei
Chuang, Po-Ya Abel

Publication Date

2018-12-07

DOI

10.1021/acscatal.8b02217

Peer reviewed

ACS Catalysis

Research Article

Cite This: ACS Catal. 2018, 8, 11688−11698

pubs.acs.org/acscatalysis

Defining Nafion Ionomer Roles for Enhancing Alkaline Oxygen Evolution Electrocatalysis

Guang-Fu Li,*,† Donglei Yang,† and Po-Ya Abel Chuang*

Department of Mechanical Engineering, University of California, Merced, California 95343, United States

Supporting Information

ABSTRACT: The electrocatalytic oxygen evolution reaction (OER) is not strictly a surface reaction, because it takes place in a thin hydrous electrical double layer (EDL). In this work, we perform an in-depth study of Nafion ionomer functions in both catalyst inks and catalyst layers (CL) for high-efficiency OER in alkaline media. Based on cyclic voltammetry results, an analysis method is developed to characterize pseudocapacitance and EDL charging capacitance independently. This enables accurate quantification of interfacial charge transport behavior and active sites for OER. Zeta potential measurements confirm that Nafion ionomer serves as a stabilizing and binding agent in catalyst−solvent inks. The data obtained from the half-cell tests in 1 M KOH reveal that increasing ionomer content in CL reduces OER performance due to higher mass transport resistance and less active sites. The sample with I/C = 1/24 (weight ratio of Nafion ionomer to IrO_x catalyst) exhibits an approximately 1.7-times higher OER activity than that of I/C = 2/1. Furthermore, the ionomer blocking effect is found to be a common phenomenon, which was observed in a wide range of catalyst loadings and three different catalyst materials. Nevertheless, as demonstrated by Nafion-free samples, the addition of Nafion is indispensable for efficient catalyst utilization. Our study shows that the optimized ionomer content in the CL is 10−30 wt % of catalyst loading. Within this range, Nafion, catalyst particles, and electrolyte solution form efficient interaction, resulting in good connectivity of the charge conduction paths without inhibiting the gas diffusion.

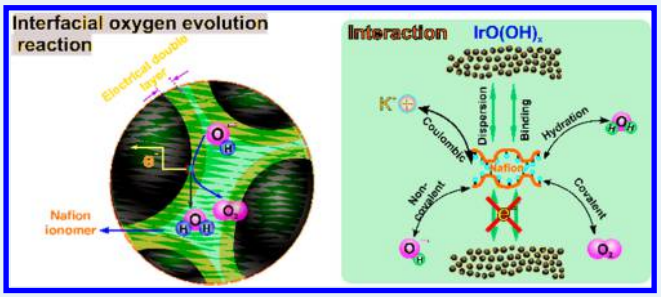

KEYWORDS: *Nafion ionomer, oxygen evolution reaction, alkaline water electrolysis, electrical double layer, iridium oxide, pseudocapacitance*

1. INTRODUCTION

Electrocatalyzing oxygen evolution reactions (OER) are critical for clean-energy storage and conversion techniques, such as water electrolysis.[1−3] Compared with hydrogen evolution reaction, the OER, taking place at the anode of an electrolysis device, is recognized as a major obstacle for commercialization in terms of efficiency, durability and cost of catalyst materials.[3−5] Industrial water splitting is generally conducted in an alkaline solution, because noticeable corrosion occurs when the process is carried out in acidic electrolytes. In alkaline media, nonprecious metals (e.g., Ni, Co, Fe, and Mo) can be used as catalyst materials, thereby providing cost reduction.[6−10] Over the last few decades, the activity and long-term stability of OER catalysts have been improved by numerous studies, as reported in several recent review articles.[1,5,11−13] However, evaluating actual catalyst performance accurately in alkaline media still remains a challenge.[14−17] Uncertainties resulting from ink preparation and deposition, measurement protocols, operating conditions, and interfacial interaction are unavoidable, which influences the validity of testing results. Minimizing these uncertainties to understand actual catalyst performance is essential for further development of efficient OER catalysts.

Thin film rotating disk (TF-RDE) and ring-disk (TF-RRDE) electrodes are the most commonly employed tools for evaluating electrocatalysts.[18−20] The obtained results can be used to predict catalyst performance in a full electrochemical cell.[21] Moreover, TF-RDE/RRDE features a built-in three-electrode system that is convenient to operate and can provide reliable testing results. Compared with conducting measurement of the full membrane electrode assembly (MEA), TF-RDE/RRDE has an advantage in saving time and materials without compromising the accuracy of catalyst performance.[20,22,23] The composition and preparation technique of a thin-film catalyst layer (CL) on the disk electrode have a significant effect on obtaining the intrinsic properties of applied materials.[19,21,24] The CL is generally fabricated by drying a uniformly deposited catalyst ink, which consists of solvent, catalyst particles, and ionomer solution. In principle, the ionomer can be integrated with metal oxide catalysts to change the form of the reaction interface and, accordingly, affect the reaction efficiency. There needs to be enough ionomer to provide good contact with the catalyst nano-

Received: June 6, 2018
Revised: September 23, 2018
Published: November 1, 2018

DOI: 10.1021/acscatal.8b02217
ACS Catal. 2018, 8, 11688−11698

particles but not so much that mass diffusion is inhibited. Extensive studies in fuel cells and electrolyzers have confirmed that 20−40 wt % ionomer in CL can achieve the highest MEA performance.[25−28] However, these optimized values for MEA cannot be directly applied to TF-RDE/RRDE systems due to different reaction conditions at the triple-phase boundaries. In particular, using an ionic ionomer in alkaline media creates unusual shifts of the transport behaviors and structure.[29,30]

Currently, the most widely used ionomer in alkaline media is DuPont's Nafion, owing to its excellent mechanical and electrochemical stability.[6,8,29,31−33] Nafion is a multifunctional copolymer composed of a Teflon-backbone and functionalized sulfonic acid side chain. Once solvated, the hydrophobic PTFE backbone and hydrophilic sulfonic acid group lead to a phase-separated structure that gives Nafion unique transport properties, e.g. remarkable cation conduction and electron or anion insulation.[29] The most common application of Nafion ionomer is for proton exchange membranes in fuel cells and water electrolyzers.[28,34−37] For TF-RDE/RRDE, Nafion primarily serves as a dispersant for catalyst ink mixing and as a binder to avoid CL detachment from the disk electrode.[19,21] The final structure of the postdrying CL is strongly influenced by interfacial interactions. In addition, the structure and transport behavior of the ionomer in a TF-RDE/RRDE system is drastically different from those in the continuous Nafion membrane due to the microstructural differences between these two materials.[38,39]

To-date, there is no in situ physicochemical characterization tool available to visualize Nafion morphology and electrochemical behaviors.[39] This presents a challenge when trying to obtain information regarding Nafion morphology and its transport behavior, even using state-of-the-art electron microscopes. The reason is that the ionomer does not display sufficient image contrast as compared with the electrocatalysts in the electron microscope.[37] The lack of direct structural observation leads to a poor understanding of ionomer-dependent reactions. Instead, electrochemical methods have gained a significant interest as a means of performing in situ studies of Nafion-related interfacial structure and electrochemical behaviors.[19] The interactions of ionomer, catalyst, reactants, products, and reaction intermedia create a very complex thin hydrous electrical double layer (EDL).[40−43] Based on our previous work, the formed EDL has a dominant influence on the OH^- coupled electron transfer reaction.[44,45] However, the role of Nafion ionomer in OER is still unclear. In this work, we focus on the impact of Nafion ionomer and its interaction with other components in EDL by applying in situ electrochemical diagnostic methods. It is expected that an improved understanding of ionomer roles can help to increase catalyst utilization and long-term stability.

2. RESULTS AND DISCUSSION

The CL used in this study is fabricated from an ink mixture consisting of commercial IrO_x catalyst, ionomer, and ethanol solvent. Based on our previous work, it is found that the IrO_x material (BET surface are = 32.5 m^2 g^{-1}) is a combination of primarily amorphous Ir oxide and a small content of Ir metal.[44,45] A schematic illustration of the CL structure and interfacial OER is shown in Figure 1. To facilitate an electron transfer Faradaic reaction, the formed CL should have the following three features: (1) uniform distribution of catalyst and ionomer to maximize catalyst utilization; (2) large active area available for OER; and (3) well-connected paths for facile

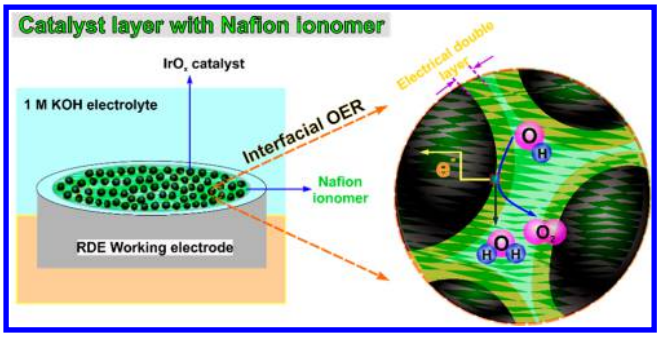

Figure 1. Schematic illustration of ionomer-containing catalyst layer and interfacial OER in alkaline media.

OH^--, electron-, and O_2-transport.[46] In addition to short-term performance, sufficient stability of the CL is necessary for long-term application. A critical aspect for alkaline OER, though not adequately studied, is the role of ionomer, which governs the ink properties and the physical and electrochemical behaviors of CLs, especially at the reaction interface (i.e., EDL). Observed from the linear scan voltammetry (LSV) in Figure S1 (refer to Supporting Information, SI), the Nafion-containing CL exhibits the highest OER activity in the alkaline medium compared to those prepared by anion ionomer As-4 (Tokuyama Corp.) and nonionic PTFE binder (Fuel Cell Store). Thus, the Nafion ionomer is selected to be studied toward the enhanced OER in this work.

2.1. Structural Characterization of Catalyst Inks and Fabricated CLs. The weight ratio of ionomer to catalyst (I/C) used in our work ranges between 0 and 2, which spans the weight ratios of most published reports.[8,19,46−49] The solid volume fraction of catalyst and ionomer particles (5 mg IrO_x dispersed in 4 mL of absolute ethanol) in the prepared ink is less than 0.5% to ensure a highly diluted solution. This minimizes the interaction between catalyst particles to achieve uniform dispersion.

Prior to deposition of CL onto RDE/RRDE, the catalyst ink is filled into a quartz cell for the zeta potential, particle size, and electric conductivity measurements. Results in Figure 2(a) clearly reveal that an increasing I/C ratio leads to a more negative zeta potential, meaning stronger electrostatic repulsion force between particles and thus enhancing ink dispersibility and stability.[50] Meanwhile, the average size of ionomer-catalyst agglomerates and electric conductivity both increase with increasing ionomer content, as shown in Figure 2(b). Compared with the ionomer-free sample, a small amount of ionomer (I/C = 1/12) can cause a noticeable increase in the hydrodynamic diameter of the particles (225 to 275 nm), which indicates the adsorption of Nafion onto catalyst particles. The electric conductivity of the ink is nearly proportional to ionomer content, confirming the charge of the SO_3^- group in the Nafion molecule.

Images taken by SEM and optical microscope are shown in Figure 3 and Figure S2 (refer to SI), respectively. The morphology of the fabricated CL has a strong dependence on ionomer content. The varying colors in optical images are caused by the interference of thin Nafion films. The ionomer-free CL forms a nonuniform distribution with large aggregates. In the I/C range of 1/24 to 1/2, the catalyst particles can disperse well as a thin ionomer film covers the CL surface. Further increasing the Nafion content results in the formation of large catalyst−ionomer agglomerates, which can block mass

DOI: 10.1021/acscatal.8b02217
ACS Catal. 2018, 8, 11688−11698

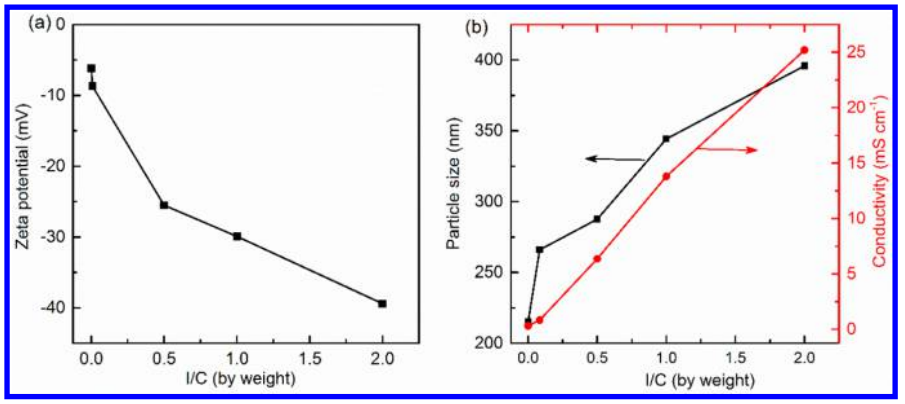

Figure 2. (a) Zeta potential and (b) particle size (left) and electric conductivity (right) of catalyst ink as a function of ionomer to catalyst ratio (I/C).

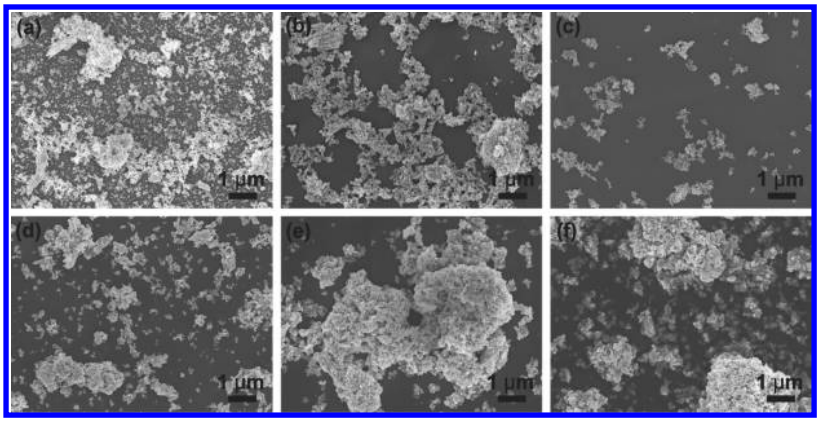

Figure 3. SEM images of IrO_x catalyst layers with various I/C ratios. (a) Nafion free, (b) I/C = 1/24, (c) I/C = 1/8, (d) I/C = 1/2, (e) I/C = 1/1, and (f) I/C = 2/1.

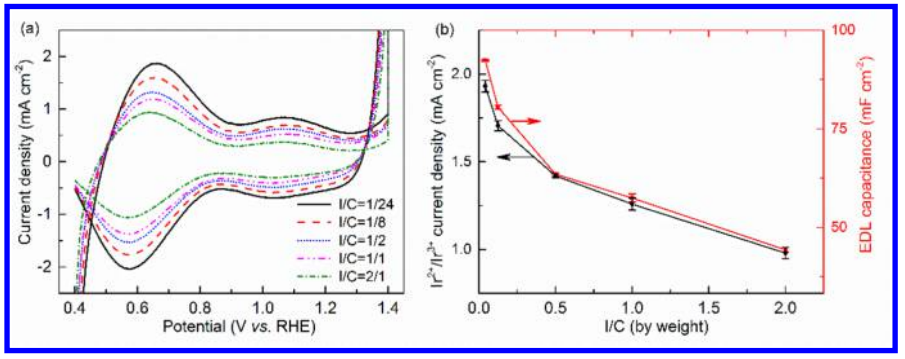

Figure 4. (a) Modified CV curves of varied I/C samples at 50 mV s^{-1}. The resulting current is the measured current subtracted by the EDL current. (b) Current density of Ir^{2+}/Ir^{3+} redox peak (left) and EDL capacitance (right) as a function of I/C ratio.

transport and cause reduction of the active area and catalyst utilization. These microimages reveal that the Nafion ionomer can serve not only as a dispersing agent to improve catalyst distribution but also as a binder to enhance the interactions between catalyst particles. Therefore, optimization of the Nafion ionomer content is required to maximize catalyst effective utilization.

2.2. Ionomer Blocking Effects on Interfacial Behaviors. In this section, the catalyst loading on the RDE is held at 0.24 mg cm^{-2}, and the weight ratio of I/C varies from 1/24 to 2/1. The electrochemical measurements are carried out in N_2-saturated 1 M KOH. First, cyclic voltammetry (CV) is conducted to study the pseudocapacitive (due to active metal redox) and capacitive (due to EDL charging) behaviors of the ionomer-containing catalysts. With regard to the Faradaic electron-transfer reaction, the characteristics of solid-state pseudocapacitive and OER are similar.[23,51,52] Therefore, investigation of pseudocapacitance can provide useful information about potential active reaction sites for OER. Nearly all exceptional electrocatalysts used for OER exhibit large pseudocapacitance.[23,48,52]

The CV spectrum in a potential range of 0.4−1.4 V can define the unique "fingerprint" features of the studied IrO_x.[40] The measured current in Figure S3 (refer to SI) results from the combination of EDL charging process and active metal redox. To isolate the effect of pseudocapacitance, CV curves within the potential range of 0.8−1.0 V are obtained. The near rectangular shape of the CV curves in Figure S4 (refer to SI)

DOI: 10.1021/acscatal.8b02217
ACS Catal. 2018, 8, 11688−11698

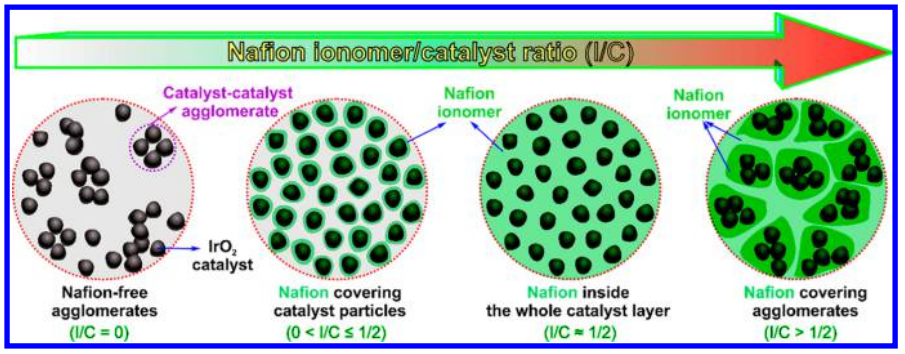

Figure 5. Schematic illustration of catalyst layer dispersion and structure as a function of I/C ratio.

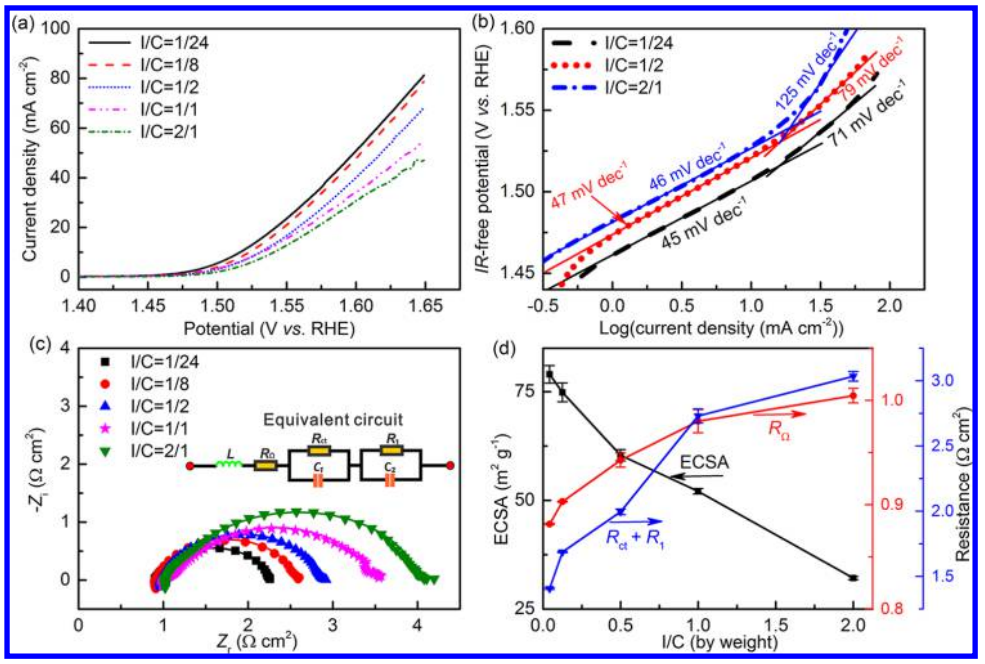

Figure 6. (a) LSV curves at a scan rate of 2 mV s^{-1}; (b) *IR*-corrected Tafel plots; (c) EIS spectra at 1.55 V. The inset is the modeled equivalent circuit. Symbols—raw data; lines—linear fit to the data; and (d) the calculated ECSA (left), and R_Ω (right 1st) and $R_{ct} + R_1$ (right 2nd).

confirms the pure non-Faradaic capacitive behavior.[53] The detected EDL current at the same scan rate (50 mV s^{-1}) is subtracted from the total current and the modified CV curves are replotted in Figure 4(a). The newly processed CV spectra exhibit only pseudocapacitive behaviors, and two reaction couples can be found at around 0.65 V (Ir^{2+}/Ir^{3+}) and 1.05 V (Ir^{3+}/Ir^{4+}). Note that the redox potential of Ir^{4+}/Ir^{5+} is higher than that of the standard OER potential.[23] The even higher oxidization states, such as Ir^{6+}, are thermodynamically unstable and cannot serve as reaction intermediates during stable OER operation.[5,48] From Figure 4(a), we clearly observe that the pseudocapacitance decreases with increasing I/C ratio, demonstrating a reduction of active sites due to ionomer coverage. Such coverage blocks electroactive intermediate (*OH, *O, and *OOH) adsorption and electron transport in the hydrous EDL.

From Figure 4(b), it is found that the pseudocapacitive current initially drops sharply for low I/C ratios (≤1/2) and then continues to decrease linearly for high I/C ratios (>1/2). This observation agrees with the particle size distribution from Figure 2(b), which suggests that ionomer/catalyst interactions reach saturation near I/C = 1/2. For low I/C samples, each ionomer molecule binds with catalyst particles to form a uniform dispersion until the entire surface of catalyst particles is covered. The continuity of charge conductivity in the CL can be impeded significantly, leading to the drastic reduction of active sites. After reaching saturation at around I/C = 1/2, adding more Nafion ionomer results in the formation of agglomerates. Based on measurements of particle hydrodynamic size in Figure 2(b), the thickness of the ionomer film covered on the agglomerate surface grows by around 50 nm with increasing I/C from 1/2 to 2/1. This leads to a linear increase in agglomerate size and a linear decrease in pseudocapacitive current. Schematic illustrations summarizing the interaction between Nafion ionomer and catalysts are shown in Figure 5.

It is well-known that the EDL charging capacitance increases in proportion to the number of electrochemical active sites.[17,54] According to the single-point CV method,[44] the EDL capacitance can be estimated by linearly fitting the scan rate-current plots. Taking the average of the absolute slope values from the anodic and cathodic sweeps, the resulting EDL capacitances in Figure 4(b) are found to be between 92.3 ± 0.2 mF cm^{-2} and 44.3 ± 0.6 mF cm^{-2} for various I/C samples. Furthermore, the EDL capacitance exhibits the same dependence on Nafion content as the observed pseudocapacitance.

DOI: 10.1021/acscatal.8b02217
ACS Catal. 2018, 8, 11688−11698

This finding indicates that both the EDL capacitance and pseudocapacitance can effectively reflect charge transport and active sites in EDL. The increase of ionomer content in CL leads to an increase of interfacial charge transport resistance and a reduction of available active sites.

The electrocatalytic OER activity is investigated by potential-controlled linear scanning voltammetry (LSV) taken at 2 mV s^{-1}. Figure 6(a) shows the LSV curves at a rotating speed of 1600 rpm. By comparing the integrated area from 1.4 to 1.65 V, the I/C = 1/24 sample has an approximately 1.7-times higher OER activity than that of I/C = 2/1 sample. In the kinetic region (10 mA cm^{-2}), the overpotential increases ~20 mV for the studied range of I/C = 1/24 to 2/1 (see Figure S5 in SI). In the kinetic-diffusion mixed region, the OER performance is affected by both kinetic and mass transport. Therefore, the overpotential has more increases with increasing Nafion content. For instance, there exists an increment of ~40 mV at 40 mA cm^{-2}.

The ionomer content-dependent activity is further analyzed using *IR*-free Tafel plots. Two Tafel slope regions could be discerned in Figure 6(b). In the range of 1−10 mA cm^{-2}, the fitted slopes are determined by transport-free reaction kinetics, since the low potential scan rate (2 mV s^{-1}) ensures minimal capacitive current and a near steady-state condition in EDLs. The Tafel slope is close to 45 mV dec^{-1} for the entire I/C range, which corresponds to the formation of surface adsorbed *O intermedia.[44,55] Thus, varying ionomer content in the CL has a negligible effect on OER kinetics. It is possible that the catalyst surface covered by a thin Nafion film can still support OER in this kinetics region. In the high current density region (30−50 mA cm^{-2}), the Tafel slope of the I/C = 1/24 sample is raised to 71 mV dec^{-1}. This indicates that the rate-limiting step falls between the initial discharge of hydroxide ions in EDL and the second electron transfer step of $*O^-$ formation according to Karsil'shchikov's pathway.[3,55] The Tafel slope remains similar when the I/C ratio is less than 1/2. In contrast, when I/C = 2/1, the fitted slope reaches 125 mV dec^{-1}, suggesting that the rate-limiting step shifts toward the initial step of hydroxide ion discharge due to the added resistances of OH^--, electron-, and O_2-transport. These added transport resistances can be mainly ascribed to the structural transition from Nafion-covered catalysts to large Nafion-filled agglomerates with increasing I/C ratio, as observed from SEM images in Figure 3. The much higher Tafel slope of the I/C = 2/1 sample also confirms that the thick ionomer film coverage on agglomerates significantly impedes mass transport and OER performance in the high current density region. Structurally, the wetted Nafion surfaces are dominated by sulfonic acid groups with only 5% of the Teflon-based backbone exposed.[56] Therefore, in addition to physical blockage of catalyst active sites, the negatively charged sulfonic acid group in Nafion can also inhibit OH^- adsorption in the EDL.

During OER, the EDL goes through a series of complicated charge accumulation, transfer, and dissipation processes.[41] Electrochemical impedance spectroscopy (EIS) with 10 mV of AC perturbation is employed as an in situ characterization tool to evaluate the interfacial behaviors in the EDL. The applied DC potential is 1.55 V, at which the OER performance of all studied samples exhibits a strong dependence on CL ionomer content, as shown in Figure 6(a). The Nyquist plots from EIS and the modeled equivalent circuit are shown in Figure 6(c). The significant variations of the impedance observed at both the high and low frequency regions indicates that ionomer content has an important influence on electron transport, reaction polarization resistance, and EDL capacitive behaviors. To quantify their contribution, EIS data are fitted by an equivalent circuit LR_Ω $(R_{ct}C_1)$ (R_1C_2), where L, R_Ω, R_{ct}, C_1, R_1, and C_2 are inductance, ohmic resistance, charge transfer resistance, EDL charging capacitance, intermediate diffusion/adsorption resistance, and capacitance, respectively.[44] This equivalent circuit is based on a two-time-constant process composed by two branches: $R_{ct}C_1$ (charge-transfer process) and R_1C_2 (surface porosity).[57,58] A constant phase element (*CPE*) is used to simulate nonideal capacitances, such as C_1 and C_2, arising from heterogeneity, surface porosity, and EDL reconstruction.[58−60] The simulated results show good agreement with the experimental data, which indicates the equivalent circuit can accurately represent the OER process occurring in the EDL.

In electrochemical measurement, catalyst activity can be quantified by ohmic resistance (R_Ω), total polarization resistance (R_{ct} + R_1), and electrochemical surface area (ECSA). The trends of these parameters as a function of ionomer loading are shown in Figure 6(d). The details for calculating ECSA based on EIS data are reported in our recently published work.[44] R_Ω consists of ohmic resistances from electronic and ionic losses and increases with increasing ionomer content. Since the ionic resistance from the electrolyte is the same for all samples, the observed increase of R_Ω confirms that Nafion ionomer inhibits electron conductivity. Meanwhile, R_{ct} + R_1 and ECSA exhibit the opposite trend with a sharp initial change followed by a nearly linear dependence on I/C. This observation is consistent with the trends of EDL capacitance and pseudocapacitance shown in Figure 4(b), indicating their similar dependency on Nafion content. Overall, adding a small amount of Nafion ionomer (I/C ≤ 1/2) to the thin-film CL causes strong ionomer/catalyst interactions and the formation of large agglomerates which, in turn, reduces ECSA and increases charge transfer resistance. In this case, the ionomer is absorbed onto the catalyst surface and the electron conductivity among the agglomerates is not hindered. That explains why only a slight reduction of R_Ω is observed when I/C increases from 1/24 to 1/8. When the Nafion ionomer content is increased further (I/C > 1/2), additional ionomers start to form layers covering the agglomerates, which become barriers for O_2, electron, and OH^- transport. The reduced OER performance indicates that the covered Nafion film hinders rapid diffusion and adsorption of reaction intermediates, such as *OH, *OOH, and *O. This can be attributed to Nafion's inability to conduct OH^- and electrons.

During OER, efficient charge- and O_2- transport in the EDL is critical in determining catalyst activity. Using TF-RRDE voltammetry allows us to quantify the contribution of each transport phenomenon. The disk potential is scanned from 1.375 to 1.60 V at 2 mV s^{-1}, while the ring potential is held at 0.4 V for detection of oxygen reduction reaction (ORR). According to our previous work,[44] the EDL charging contribution can be accurately monitored in the low overpotential region, where most generated oxygen can be detected by the ring electrode. While in the high potential mixed kinetic-diffusion region, current mainly arises from the Faradaic OER. The O_2 transport efficiency can be calculated accurately by subtracting the EDL charging current from the total disk current.

DOI: 10.1021/acscatal.8b02217
ACS Catal. 2018, 8, 11688−11698

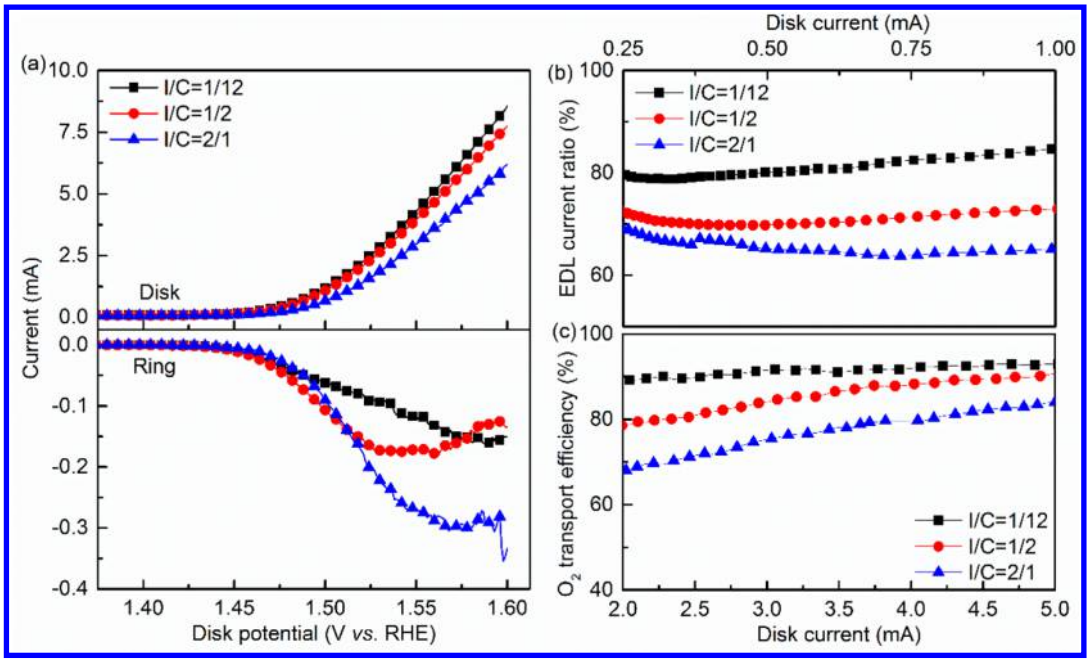

Figure 7. (a) TF-RRDE voltammetry in N_2-saturated 1 M KOH at the disk electrode (with a scan rate of 2 mV s^{-1}) and ring electrode (holding at 0.4 V). (b) EDL capacitive current ratio and (c) O_2 transport efficiency as a function of disk current.

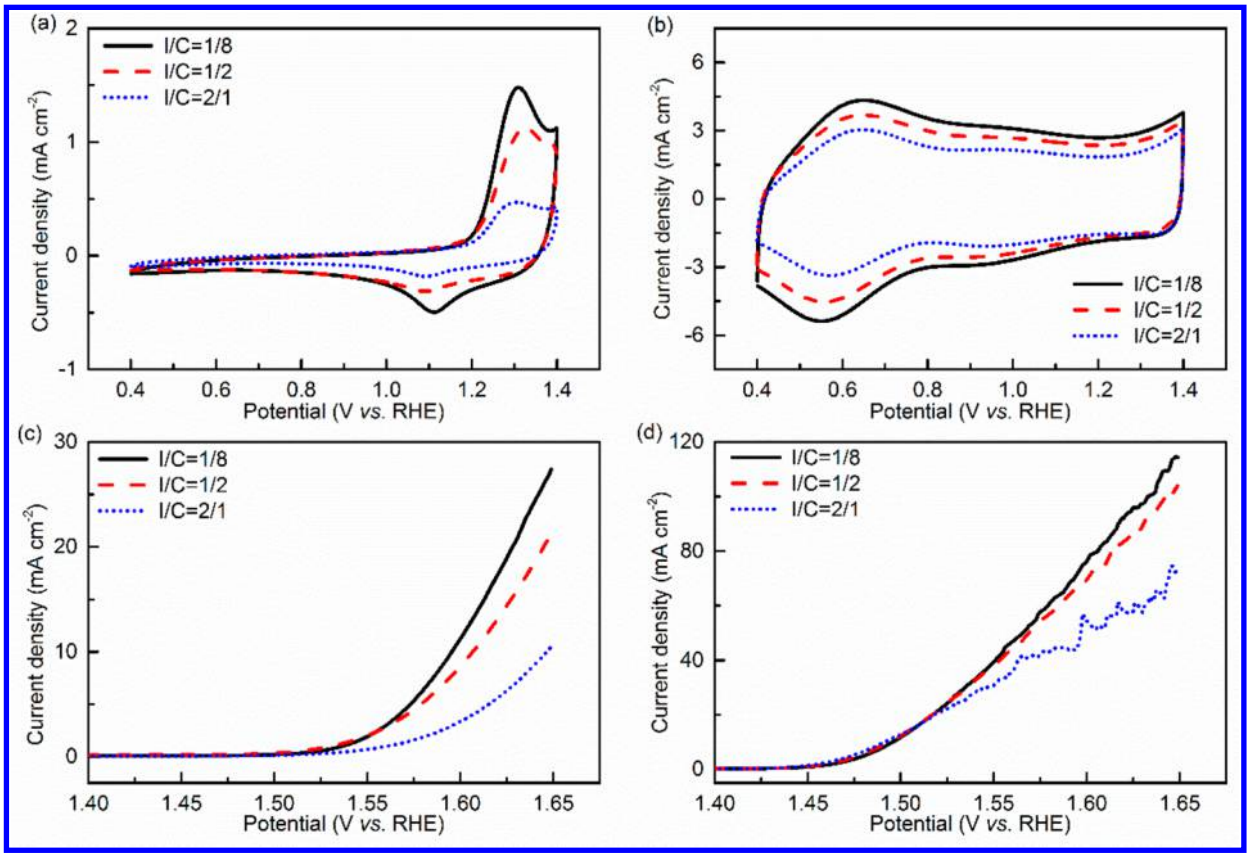

Figure 8. CV curves of (a) commercial $NiCo_2O_3$ and (b) homemade IrO_2, and LSV curves of (c) commercial $NiCo_2O_3$ and (d) homemade IrO_2 with various I/C ratios. Measurement conditions: N_2-saturated 1 M KOH, 50 mV s^{-1} for CV, 2 mV s^{-1} for LSV, 0.24 mg cm^{-2} catalyst loading and room temperature.

The TF-RRDE voltammetry data with varied I/C ratios are plotted in Figure 7(a). In the absence of OER, all the measured current at disk is from EDL capacitive and/or solid-state pesudocapacitive behaviors. The onset potential of OER is observed to be around 1.45 V, where the ORR current at the ring begins to rise. This indicates that the ring successfully detects O_2 generation from the disk. As the applied potential increases, the ring current gradually reaches a plateau,

DOI: 10.1021/acscatal.8b02217
ACS Catal. 2018, 8, 11688−11698

indicating mass transport limitation at the ring due to the saturation of O_2 transported from the disk. It is noticeable that an increasing I/C ratio decreases disk current but increases ring current. To further study this effect, RRDE data are processed at the low and high disk current regions to obtain the EDL charging current ratio and oxygen transport efficiency, respectively.[44] The results in Figure 7(b) show that increasing Nafion content in the thin-film leads to a reduction of EDL capacitive current ratio, confirming that the Nafion ionomer blocks charge transport. In the high disk current region, O_2 transport efficiency represents the percentage of O_2 leaving the EDL to the bulk electrolyte without being detected by the ring.[44] As shown in Figure 5(c), higher I/C ratios result in lower O_2 transport efficiency, which in turn, reduces OER performance. The Nafion ionomer that covers the catalyst surface can thus be proposed to block oxygen transport.

To validate the Nafion roles for efficient OER, the effect of catalyst loading and different catalyst materials is studied by the TF-RDE method. The CV and LSV results from two additional IrO_x loadings, i.e. 0.08 mg cm^{-2} and 0.48 mg cm^{-2} (Figure S6 in SI) and two different catalyst materials, commercial $NiCo_2O_3$ and homemade IrO_2 (Figure 8) confirm similar Nafion blocking effect. The BET surface area of the commercial $NiCo_2O_3$ and homemade IrO_2 is 25 m^2 g^{-1} and 70 m^2 g^{-1}, respectively.[44,45,48] The homemade IrO_2 has outstanding OER activity in 1 M KOH, e.g. 260 mV overpotential at 10 mA cm^{-2}, which has around 2-times higher OER activity than that of the commercial IrO_x. Nevertheless, the adverse effect of increasing ionomer connect can still be observed from Figure 8(d). These findings confirm that the Nafion blocking effect on mass transport and electrochemical reactions can be considered as a common phenomenon for alkaline OER regardless of catalyst loadings and materials.

2.3. Indispensable Roles of Ionomer on Efficient Catalyst Utilization and Stability. From the presented TF-RDE/RRDE results, we successfully quantify the adverse effect of Nafion on ECSA, O_2 and charge transports, and electrocatalytic OER. These results indicate that optimal OER performance can be achieved by completely eliminating Nafion ionomer in CL. To validate this hypothesis, Nafion-free samples with varied IrO_x loadings are tested in the TF-RDE system and the measurement data are directly compared to I/C = 1/2 samples. The calculated EDL capacitance as a function of IrO_x catalyst loading is shown in Figure 9. While some catalyst loss of Nafion-free samples at high loading ($\geq$0.32 mg cm^{-2}) is observed in our experiments, the trend of the EDL capacitance is validated by multiple repeated tests. The results clearly indicate that adding Nafion improves the EDL charging behavior, especially at a higher catalyst loading, due to Nafion's bonding effect. Without the ionomer, IrO_x particles have poor connectivity, which results in a higher resistance to charge transport and reduced active sites. The linear trend observed from Nafion-containing samples indicates minimal catalyst loss from the disk electrode and negligible active site overlapping.

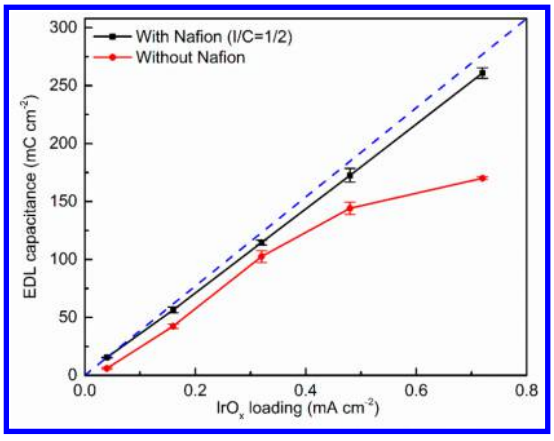

Figure 9. EDL capacitance as a function of IrO_x loading.

The observations of various IrO_x loadings in Figure S7 in SI and Figure 10 both demonstrate the presence of Nafion enhances the effective utilization of OER catalyst at both low and high specific current densities. However, the potential difference between I/C = 1/2 samples and Nafion-free samples decreases with increasing catalyst loading, especially at the high specific current density (Figure 10). This can be attributed to the Nafion blocking effects on O_2-, electron-, and OH^--transport in EDL as reported in the above observations. Thus, the overall comparison between Nafion-containing and Nafion-free samples reveals that Nafion ionomer with proper content not only prevents catalyst detachment but also facilitates the formation of an efficient interface for charge transport and OER.

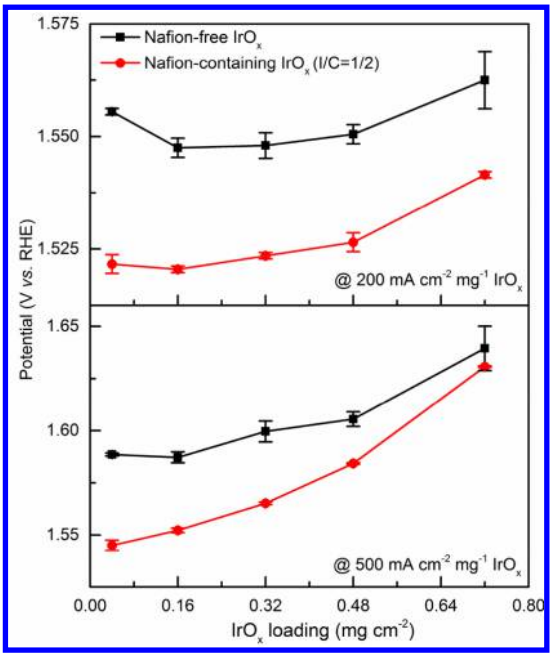

Figure 10. Comparison of OER performance and catalyst efficient utilization as a function of IrO_x loading.

In addition, the catalyst stability is investigated by conducting chronoamperometry (CA) with repeating double-potential steps in 1 M KOH for 2 h. During the CA measurement, each potential hold is 60 s and the detail potential profile can be found in Figure 11(a). Followed by the high potential (i.e 1.55 V) step, the potential decreases to 1.45 V where the OER current is minimal. At low potential, the O_2 produced at high potential can be removed efficiently during the 60 s hold time. The average current density at every high-potential step is calculated and shown in Figure 11(b). To different extents, the performance degradation can be observed for all I/C ratios over the entire measurement period. By

DOI: 10.1021/acscatal.8b02217
ACS Catal. 2018, 8, 11688−11698

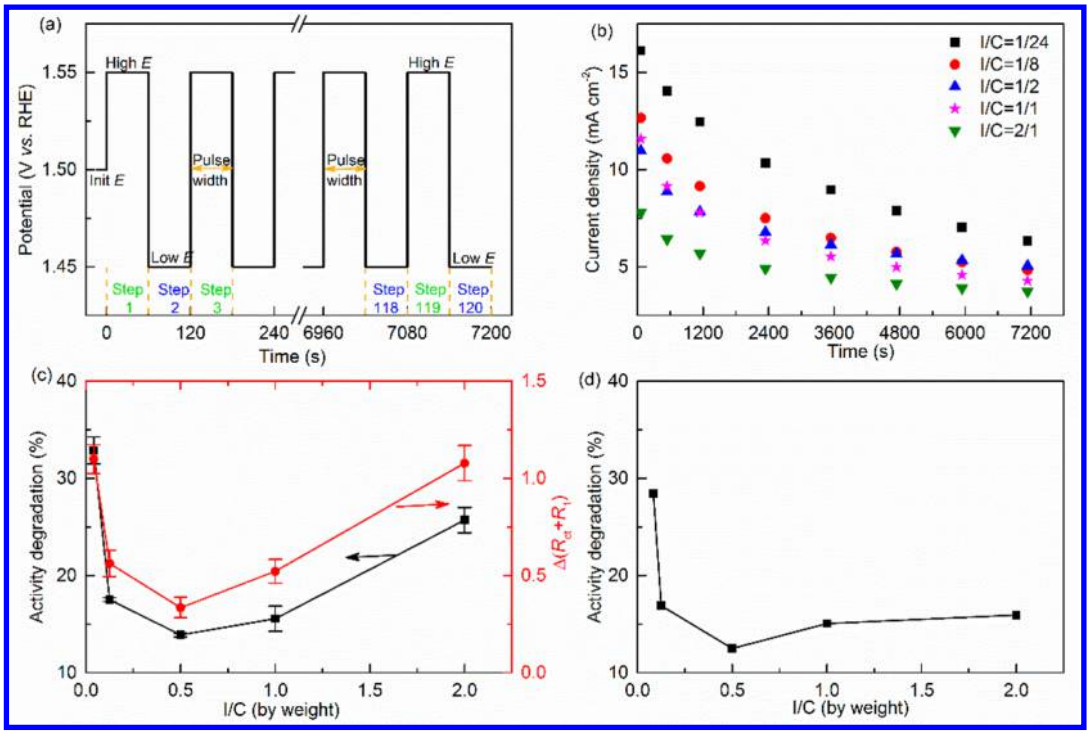

Figure 11. Stability evaluation as a function of I/C ratio. (a) Diagram of CA with major experimental parameters, (b) average current density in the high potential step of 1.55 V, (c) activity degradation and increase of total polarization resistance (R_{ct} + R_1) after 2-h CA, and (d) activity degradation after 10,000 cycles.

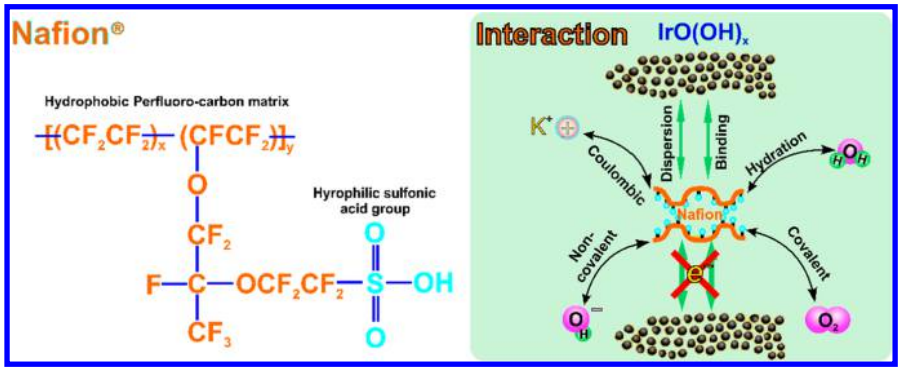

Figure 12. Schematic illustration of Nafion chemical structure and interfacial interactions with Nafion ionomer in alkaline OER.

comparing initial and ending LSV (Figure S8(a) in SI), the activity losses ($\Delta_{activity}$) can be calculated by

$$\Delta_{activity} = \frac{S_1 - S_2}{S_1} \times 100\% \quad (1)$$

where S_1 and S_2 are the integrated LSV area before and after stability tests, respectively. For all samples as shown in Figure 11(c), the trend of activity loss agrees well with the increase of total polarization resistance obtained from the Supporting Information (Figure S8(b)). To achieve maximum catalyst stability for long-term OER, the optimal I/C ratio is observed to be 1/2. Adding Nafion as a binder to the CL improves the connectivity among catalyst particles and prevents catalyst loss during the stability tests. However, excessive ionomer content results in a significant blockage of mass transport and active sites. Therefore, the chemical and structural reconstruction of EDL during the continuous stability tests can lead to the acceleration of irreversible degradation for OER performance.

Meanwhile, we also study the stability of EDL charging by repeating CV tests in O_2 saturated 1 M KOH between 0.8 and 1.0 V at 100 mV s^{-1}. The rectangular-like shape observed in Figure S9 (refer to SI) indicates reversibility of the EDL charging behavior within the applied potential range. After 10,000 cycles, the I/C = 1/2 sample in Figure 11(d) also exhibits the lowest performance loss, which is consistent with CA results. This observation demonstrates that the stability of OER catalysts can be evaluated by running durability tests at the OER potential or in the EDL charge region.

2.4. Mechanistic Illustration of Nafion Ionomer Function. As illustrated in Figure 12, Nafion ionomer is a sulfonated Teflon fluoropolymer-copolymer.[31,38] The ionomer network inside the CL has a significant effect on electrode structure, transport properties, and catalyst utilization.[37,39] When the Nafion-bonded CL is submerged in electrolyte solution, phase separation occurs, which can improve mass transport properties, e.g. cation conductivity, and electron or anion rejection.[29,59] The Nafion polymer can self-orient into a

DOI: 10.1021/acscatal.8b02217
ACS Catal. 2018, 8, 11688−11698

structure of a perfluorinated backbone core with sulfonic acid groups exposed on the outer surface. This structural and chemical reconstruction takes place during continuous electrochemical measurements, which in turn, affects OER performance. In the alkaline medium, the sulfonic acid groups are neutralized, which changes the function of the ionomer from that under the acidic condition. The efficient adsorption of aqueous OH^- onto catalyst surfaces is required for high-efficiency and for stable electrochemical reactions to take place. Nafion ionomer inside the catalyst layer can improve catalyst dispersion and prevents catalyst losses. However, the interactions of sulfonic acid/catalyst/water form a hydrophilic cluster surrounded by Teflon "inactive" regions, leading to a reduction in the number of electron and OH^- conductive pathways.[29] The catalyst active sites can thus be isolated from reactions due to Nafion coverage.

Coulombic attraction forces can drive K^+ into the OH^- absorbed reaction interface with the aid of dynamic solvation of the sulfonic acid groups (SO_3^-). The charge balance in EDL can thus be achieved. Meanwhile, the hydrophobic perfluorinated backbone provides strong adhesion to catalyst particles due to their polymer properties and proposes as a barrier to the OH^-, electron, and O_2 transports.[60] Our results demonstrate that the presence of a thin Nafion ionomer film covering the catalyst particles is required for constructing a stable and high-performance CL. For a low I/C, Nafion covers the catalyst surface and improves the catalyst dispersion and distribution. A high I/C leads to the increased aggregation of Nafion and forms a thicker ionomer layer, which has an adverse effect on mass transport and electrocatalytic OER. Therefore, there exists an optimized ionomer content range that can not only provide an efficient pathway for OH^-, electron, and O_2 transports but also form a stable reaction interface for long-term operation.

3. CONCLUSIONS

In summary, we have evaluated the effect of Nafion ionomer in CL using both in-situ and ex-situ tools and demonstrated the important roles it plays to enhance OER activity and stability in alkaline media. It is found that Nafion serves as an efficient agent for stabilizing catalyst ink as well as for binding and dispersing catalyst particles on a RDE/RRDE disk electrode. In addition, we successfully decouple the EDL charging capacitive and pseudocapacitive behaviors, which provides new insights into the relationship between Nafion and EDL structure. The presence of an optimized Nafion content is necessary to form a stable and efficient CL. Adding too much Nafion ionomer has a blocking effect on interfacial mass transport and active sites. In contrast, completely removing Nafion ionomer from the CL results in poor OER activity due to poor dispersion and connectivity of catalyst particle, especially at high catalyst loading (>0.32 mg cm^{-2}). Stability Tests including 2-h CA and 10,000 cycles of CV exhibit significant catalyst degradation for samples with low Nafion content (I/C < 1/8). On the other hand, a high I/C leads to the increased aggregation of Nafion and a thicker ionomer layer, which has an adverse effect on mass transport and electrocatalytic OER reaction. The OER activity has a reduction of 40% when the I/C ratio increases from 1/24 to 2/1. The optimal I/C ratio for achieving high OER activity and stability ranges from 1/8 to 1/2. In this range, well-organized ionomer networks in the CL can be formed with superior electrochemical stability and minimal reduction of OER performance.

4. EXPERIMENTAL SECTION

4.1. Ink Formulation and Thin-Film Catalyst Layer Preparation. In our TF-RDE/RRDE tests, thin catalyst film is uniformly deposited onto the clean disk electrode. Details of the CL preparation can be found in our recent study.[44] Typically, iridium dioxide (≥99.99%, Alfa Aesar), Nafion solution (5 wt %, equivalent weight = 1000), and anhydrous ethanol (≥95%, Sigma-Aldrich) are used to prepare inks. The ink mixture is placed in a water-filled ultrasonic bath for 30 min to uniformly disperse catalyst particles. The temperature of the sonication bath is closely monitored not to exceed 35 °C. The studied ionomer to catalyst weight ratios (I/C) are 1/24, 1/8, 1/2, 1/1, and 2/1 with an IrO_x loading of 0.24 mg cm^{-2}. For the Nafion free experiment, a wide range of catalyst loadings (0.08−0.72 mg cm^{-2}) are studied and the results are directly compared to samples with I/C = 1/2.

4.2. Structural Characterization. After 30 min of sonication, the well-dispersed catalyst ink is filled in a quartz cell for zeta-potential, particle size, and electric conductivity measurements on a Malvern Zetasizer Nano ZS90 at room temperature. The SEM images are taken by Zeiss Field Emission Gemini SEM 500 at 5 kV. For all SEM samples, the IrO_x catalyst with 0.24 mg cm^{-2} is deposited on a silicon wafer. The microscopic images of the thin-film CLs prepared in the RDE are obtained by Leica DM 2500 M equipped with the MC 120HD camera.

4.3. Electrochemical Tests. The electrochemical tests are conducted with a bipotentiostat (CHI 750E) at room temperature and ambient pressure. A standard three-electrode system is set up with a Hg/HgO (filled in 1 M KOH), a platinum wire (7 mm OD × 65 mm), and a RDE/RRDE as reference electrode, counter electrode, and working electrode, respectively. More specifically, the RDE (E3, Pine Instrument Co.) with a glass carbon (GC, 5 mm OD) and the RRDE (E7R9, Pine Instrument Co.) with a submillimeter gap between its GC disk (5.61 mm OD) and platinum ring (7.92 mm OD, 6.25 mm ID) are employed as the working electrode in TF-RDE/RRDE measurements. Based on the reversible hydrogen electrode (RHE), the calibrated potential of the applied Hg/HgO reference electrode in 1 M KOH and at room temperature is 0.898 V. The three-electrode system is immersed in a 300 mL PTFE cell filled with N_2-saturated 1 M KOH (pH = 13.93) as the electrolyte solution.

Prior to depositing catalyst inks, the working electrode is carefully polished with Al_2O_3 (50 nm) suspension on a piece of rayon microcloth for 2−3 min followed by rinsing with DI water. A drop of the ink sample is then dropped onto the entire GC surface via a 2−20 mL adjustable micropipette and dried under a 600 W infrared lamp. The coating and drying process are repeated until the targeted loading is reached. Then, the working electrode is mounted onto a modulated speed rotator assembly (Pine Research Instrumentation, Inc.) and immersed in the electrolyte-filled PTFE cell with the coated CL facing downward.

The benchmarked test protocols and parameters of TF-RDE and TF-RRDE are established in our previous work.[44] In summary, stationary CV (0 rpm), standard LSV, EIS, and CA (1600 rpm) are performed in TF-RDE to evaluate the effect of Nafion ionomer. The Nyquist spectra are analyzed with the aid of CHI software. As for the stability assessment, 10,000 CV cycles from 0.8 to 1.0 V are performed at 100 mV s^{-1} and 200 rpm, and the electrolyte solution is saturated with O_2. In TF-

DOI: 10.1021/acscatal.8b02217
ACS Catal. 2018, 8, 11688−11698

RRDE tests, standard voltammetry tests are conducted with a rotating speed of 1600 rpm, to demonstrate the influence of Nafion on the EDL charging process and O_2 transport efficiency during OER. The disk potential increases linearly with time, while the ring potential is held at 0.4 V for oxygen reduction reaction. The collection efficiency of our applied RRDE is determined to be 37.3% by detecting the redox couple $[Fe(CN)_6]^{3-}/[Fe(CN)_6]^{4-}$. All potentials reported in this work are presented in reference to RHE.

■ ASSOCIATED CONTENT

Supporting Information

The Supporting Information is available free of charge on the ACS Publications website at DOI: 10.1021/acscatal.8b02217.

LSV curves of IrO_x catalyst layer with various ionomers; optical microscopic images; CV curves between 0.4 and 1.4 V; CV curves regarding EDL charging capacitive behaviors; potential dependence on I/C; loading effects, and stability tests. (PDF)

■ AUTHOR INFORMATION

Corresponding Authors

*E-mail: gli27@ucmerced.edu.

*E-mail: abel.chuang@ucmerced.edu.

ORCID

Po-Ya Abel Chuang: 0000-0002-0440-1974

Author Contributions

†G.L. and D.Y. contributed equally to this work.

Notes

The authors declare no competing financial interest.

■ ACKNOWLEDGMENTS

The authors would like to thank Ashlie Martini for reviewing our work and Malvern Panalytical for loaning us the Zetasizer. This work is supported by GREENPower Program (IIID 2015-09) from Commission on Higher Education - Philippine California Advanced Research Institutes (CHED-PCARI) of the Republic of the Philippines.

■ REFERENCES

(1) Suen, N.-T.; Hung, S.-F.; Quan, Q.; Zhang, N.; Xu, Y.-J.; Chen, H. M. Electrocatalysis for the oxygen evolution reaction: recent development and future perspectives. *Chem. Soc. Rev.* **2017**, *46*, 337−365.

(2) Hunter, B. M.; Gray, H. B.; Müller, A. M. Earth-Abundant Heterogeneous Water Oxidation Catalysts. *Chem. Rev.* **2016**, *116*, 14120−14136.

(3) Doyle, R. L.; Lyons, M. E. G. The Oxygen Evolution Reaction: Mechanistic Concepts and Catalyst Design. In *Photoelectrochemical Solar Fuel Production: From Basic Principles to Advanced Devices*; Giménez, S., Bisquert, J., Eds.; Springer International Publishing: Cham, 2016; pp 41−104.

(4) Chen, Y.; Mojica, F.; Li, G.; Chuang, P.-Y. A. Experimental study and analytical modeling of an alkaline water electrolysis cell. *Int. J. Energy Res.* **2017**, *41*, 2365−2373.

(5) Spoeri, C.; Kwan, J. T. H.; Bonakdarpour, A.; Wilkinson, D.; Strasser, P. The Stability Challenges of Oxygen Evolving Catalysts: Towards a Common Fundamental Understanding and Mitigation of Catalyst Degradation. *Angew. Chem., Int. Ed.* **2017**, *56*, 5994−6021.

(6) Mefford, J. T.; Rong, X.; Abakumov, A. M.; Hardin, W. G.; Dai, S.; Kolpak, A. M.; Johnston, K. P.; Stevenson, K. J. Water electrolysis on La1-xSrxCoO3-[delta] perovskite electrocatalysts. *Nat. Commun.* **2016**, *7*, 11053.

(7) Burke, M. S.; Enman, L. J.; Batchellor, A. S.; Zou, S.; Boettcher, S. W. Oxygen Evolution Reaction Electrocatalysis on Transition Metal Oxides and (Oxy)hydroxides: Activity Trends and Design Principles. *Chem. Mater.* **2015**, *27*, 7549−7558.

(8) Diaz-Morales, O.; Ledezma-Yanez, I.; Koper, M. T. M.; Calle-Vallejo, F. Guidelines for the Rational Design of Ni-Based Double Hydroxide Electrocatalysts for the Oxygen Evolution Reaction. *ACS Catal.* **2015**, *5*, 5380−5387.

(9) Gong, M.; Dai, H. A mini review of NiFe-based materials as highly active oxygen evolution reaction electrocatalysts. *Nano Res.* **2015**, *8*, 23−39.

(10) Xu, J.; Sousa, J. P. S.; Mordvinova, N. E.; Costa, J. D.; Petrovykh, D. Y.; Kovnir, K.; Lebedev, O. I.; Kolen'ko, Y. V. Al-Induced In Situ Formation of Highly Active Nanostructured Water-Oxidation Electrocatalyst Based on Ni-Phosphide. *ACS Catal.* **2018**, *8*, 2595−2600.

(11) Hong, W. T.; Risch, M.; Stoerzinger, K. A.; Grimaud, A.; Suntivich, J.; Shao-Horn, Y. Toward the rational design of non-precious transition metal oxides for oxygen electrocatalysis. *Energy Environ. Sci.* **2015**, *8*, 1404−1427.

(12) Trotochaud, L.; Boettcher, S. W. Precise oxygen evolution catalysts: Status and opportunities. *Scr. Mater.* **2014**, *74*, 25−32.

(13) Fabbri, E.; Habereder, A.; Waltar, K.; Kotz, R.; Schmidt, T. J. Developments and perspectives of oxide-based catalysts for the oxygen evolution reaction. *Catal. Sci. Technol.* **2014**, *4*, 3800−3821.

(14) Ganassin, A.; Maljusch, A.; Colic, V.; Spanier, L.; Brandl, K.; Schuhmann, W.; Bandarenka, A. Benchmarking the Performance of Thin-Film Oxide Electrocatalysts for Gas Evolution Reactions at High Current Densities. *ACS Catal.* **2016**, *6*, 3017−3024.

(15) McCrory, C. C.; Jung, S.; Ferrer, I. M.; Chatman, S. M.; Peters, J. C.; Jaramillo, T. F. Benchmarking hydrogen evolving reaction and oxygen evolving reaction electrocatalysts for solar water splitting devices. *J. Am. Chem. Soc.* **2015**, *137*, 4347−4357.

(16) Costentin, C.; Passard, G.; Savéant, J.-M. Benchmarking of Homogeneous Electrocatalysts: Overpotential, Turnover Frequency, Limiting Turnover Number. *J. Am. Chem. Soc.* **2015**, *137*, 5461−5467.

(17) McCrory, C. C. L.; Jung, S.; Peters, J. C.; Jaramillo, T. F. Benchmarking heterogeneous electrocatalysts for the oxygen evolution reaction. *J. Am. Chem. Soc.* **2013**, *135*, 16977−16987.

(18) Stonehart, P.; Ross, P. N. The use of porous electrodes to obtain kinetic rate constants for rapid reactions and adsorption isotherms of poisons. *Electrochim. Acta* **1976**, *21*, 441−445.

(19) Shinozaki, K.; Zack, J. W.; Pylypenko, S.; Pivovar, B. S.; Kocha, S. S. Oxygen Reduction Reaction Measurements on Platinum Electrocatalysts Utilizing Rotating Disk Electrode Technique: II. Influence of Ink Formulation, Catalyst Layer Uniformity and Thickness. *J. Electrochem. Soc.* **2015**, *162*, F1384−F1396.

(20) Shao, M.; Chang, Q.; Dodelet, J.-P.; Chenitz, R. Recent Advances in Electrocatalysts for Oxygen Reduction Reaction. *Chem. Rev.* **2016**, *116*, 3594−3657.

(21) Kocha, S. S.; Garsany, Y.; Myers, D. *Testing Oxygen Reduction Reaction Activity with the Rotating Disc Electrode Technique*; NREL: DOE, 2013.

(22) Lee, S.-J.; Pyun, S.-I.; Lee, S.-K.; Kang, S.-J. L. Fundamentals of Rotating Disc and Ring−Disc Electrode Techniques and their Applications to Study of the Oxygen Reduction Mechanism at Pt/C Electrode for Fuel Cells. *Isr. J. Chem.* **2008**, *48*, 215−228.

(23) Eftekhari, A. From pseudocapacitive redox to intermediary adsorption in oxygen evolution reaction. *Mater. Today Chem.* **2017**, *4*, 117−132.

(24) Holdcroft, S. Fuel Cell Catalyst Layers: A Polymer Science Perspective. *Chem. Mater.* **2014**, *26*, 381−393.

(25) Nogueira Bonifacio, R.; Oliveira Neto, A.; Linardi, M. Comparative analysis between mass and volume of catalysts as a criterion to determine the optimal quantity of Nafion ionomer in catalyst layers. *Int. J. Hydrogen Energy* **2015**, *40*, 2840−2849.

(26) Sasikumar, G.; Ihm, J. W.; Ryu, H. Dependence of optimum Nafion content in catalyst layer on platinum loading. *J. Power Sources* **2004**, *132*, 11−17.

(27) Li, B.; Qiao, J.; Yang, D.; Lin, R.; Lv, H.; Wang, H.; Ma, J. Effect of metal particle size and Nafion content on performance of MEA using Ir-V/C as anode catalyst. *Int. J. Hydrogen Energy* **2010**, *35*, 5528−5538.
(28) Wuttikid, K.; Shimpalee, S.; Weidner, J. W.; Punyawudho, K. Evaluation of Nafion with Various Pt-C Concentrations in Membrane Electrode Assemblies for PEMFCs. *Fuel Cells* **2017**, *17*, 643−651.
(29) Kusoglu, A.; Weber, A. Z. New Insights into Perfluorinated Sulfonic-Acid Ionomers. *Chem. Rev.* **2017**, *117*, 987−1104.
(30) Buckley, D. N.; Burke, L. D.; Mulcahy, J. K. The oxygen electrode. Part 7.-Influence of some electrical and electrolyte variables on the charge capacity of iridium in the anodic region. *J. Chem. Soc., Faraday Trans. 1* **1976**, *72*, 1896−1902.
(31) Mauritz, K. A.; Moore, R. B. State of Understanding of Nafion. *Chem. Rev.* **2004**, *104*, 4535−4586.
(32) Suntivich, J.; May, K. J.; Gasteiger, H. A.; Goodenough, J. B.; Shao-Horn, Y. A perovskite oxide optimized for oxygen evolution catalysis from molecular orbital principles. *Science* **2011**, *334*, 1383−1385.
(33) Yeo, R. S.; McBreen, J.; Kissel, G.; Kulesa, F.; Srinivasan, S. Perfluorosulphonic acid (Nafion) membrane as a separator for an advanced alkaline water electrolyser. *J. Appl. Electrochem.* **1980**, *10*, 741−747.
(34) Sapountzi, F. M.; Divane, S. C.; Papaioannou, E. I.; Souentie, S.; Vayenas, C. G. The role of Nafion content in sputtered IrO2 based anodes for low temperature PEM water electrolysis. *J. Electroanal. Chem.* **2011**, *662*, 116−122.
(35) Liu, L.; Chen, W.; Li, Y. An overview of the proton conductivity of nafion membranes through a statistical analysis. *J. Membr. Sci.* **2016**, *504*, 1−9.
(36) Jung, H.-Y.; Choi, J.-H. The effect of a modified Nafion binder on the performance of a unitized regenerative fuel cell (URFC). *J. Solid State Electrochem.* **2012**, *16*, 1571−1576.
(37) Lopez-Haro, M.; Guetaz, L.; Printemps, T.; Morin, A.; Escribano, S.; Jouneau, P. H.; Bayle-Guillemaud, P.; Chandezon, F.; Gebel, G. Three-dimensional analysis of Nafion layers in fuel cell electrodes. *Nat. Commun.* **2014**, *5*, 5229.
(38) Eastman, S. A.; Kim, S.; Page, K. A.; Rowe, B. W.; Kang, S.; Soles, C. L.; Yager, K. G. Effect of Confinement on Structure, Water Solubility, and Water Transport in Nafion Thin Films. *Macromolecules* **2012**, *45*, 7920−7930.
(39) Zhang, X.-y.; Ding, Y.-h. Thickness-dependent structural and transport behaviors in the platinum-Nafion interface: a molecular dynamics investigation. *RSC Adv.* **2014**, *4*, 44214−44222.
(40) Bard, A. J.; Faulkner, L. R. *Electrochemical Methods. Fundamentals and Applications*, 2nd ed.; John Wiley & Sons, Inc.: 2001.
(41) Bae, J. H.; Han, J.-H.; Chung, T. D. Electrochemistry at nanoporous interfaces: new opportunity for electrocatalysis. *Phys. Chem. Chem. Phys.* **2012**, *14*, 448−463.
(42) Chakhalian, J.; Millis, A. J.; Rondinelli, J. Whither the oxide interface. *Nat. Mater.* **2012**, *11*, 92−94.
(43) Strmcnik, D.; Kodama, K.; van der Vliet, D.; Greeley, J.; Stamenkovic, V. R.; Marković, N. M. The role of non-covalent interactions in electrocatalytic fuel-cell reactions on platinum. *Nat. Chem.* **2009**, *1*, 466.
(44) Li, G.; Anderson, L.; Chen, Y.; Pan, M.; Abel Chuang, P.-Y. New insights into evaluating catalyst activity and stability for oxygen evolution reactions in alkaline media. *Sustain Energy Fuels* **2018**, *2*, 237−251.
(45) Li, G.; Chuang, P.-Y. A. Identifying the forefront of electrocatalytic oxygen evolution reaction: Electronic double layer. *Appl. Catal., B* **2018**, *239*, 425−432.
(46) Bladergroen, B.; Su, H.; Pasupathi, S.; Linkov, V. Overview of membrane electrode assembly preparation methods for solid polymer electrolyte electrolyzer. In *Electrolysis*; Linkov, V., Ed.; InTech: 2012; pp 45−60.
(47) Reier, T.; Oezaslan, M.; Strasser, P. Electrocatalytic Oxygen Evolution Reaction (OER) on Ru, Ir, and Pt Catalysts: A Comparative Study of Nanoparticles and Bulk Materials. *ACS Catal.* **2012**, *2*, 1765−1772.
(48) Li, G.; Yu, H.; Wang, X.; Sun, S.; Li, Y.; Shao, Z.; Yi, B. Highly effective IrxSn1-xO2 electrocatalysts for oxygen evolution reaction in the solid polymer electrolyte water electrolyser. *Phys. Chem. Chem. Phys.* **2013**, *15*, 2858−2866.
(49) Zhang, Y.-Q.; Li, M.; Hua, B.; Wang, Y.; Sun, Y.-F.; Luo, J.-L. A strongly cooperative spinel nanohybrid as an efficient bifunctional oxygen electrocatalyst for oxygen reduction reaction and oxygen evolution reaction. *Appl. Catal., B* **2018**, *236*, 413−419.
(50) Hunter, R. J. *Zeta potential in colloid science: principles and applications*; Academic press: 2013; Vol. 2.
(51) Eftekhari, A.; Mohamedi, M. Tailoring pseudocapacitive materials from a mechanistic perspective. *Materials Today Energy* **2017**, *6*, 211−229.
(52) Liu, W.-J.; Hu, X.; Li, H.-C.; Yu, H.-Q. Pseudocapacitive Ni-Co-Fe Hydroxides/N-Doped Carbon Nanoplates-Based Electrocatalyst for Efficient Oxygen Evolution. *Small* **2018**, *14*, 1801878.
(53) Costentin, C.; Porter, T. R.; Savéant, J.-M. Conduction and reactivity in heterogeneous-molecular catalysis: New insights in water oxidation catalysis by phosphate cobalt oxide films. *J. Am. Chem. Soc.* **2016**, *138*, 5615−5622.
(54) Ardizzone, S.; Fregonara, G.; Trasatti, S. Inner and outer active surface of RuO_2 electrodes. *Electrochim. Acta* **1990**, *35*, 263−267.
(55) Matsumoto, Y.; Sato, E. Electrocatalytic properties of transition metal oxides for oxygen evolution reaction. *Mater. Chem. Phys.* **1986**, *14*, 397−426.
(56) Hiesgen, R.; Helmly, S.; Galm, I.; Morawietz, T.; Handl, M.; Friedrich, K. Microscopic Analysis of Current and Mechanical Properties of Nafion® Studied by Atomic Force Microscopy. *Membranes* **2012**, *2*, 783.
(57) He, C.; Tao, J. Three-dimensional hollow porous Co6Mo6C nanoframe as an highly active and durable electrocatalyst for water splitting. *J. Catal.* **2017**, *347*, 63−71.
(58) Li, H.; Chen, Z.; Yu, Q.; Zhu, W.; Cui, W. Effects of Tungsten Carbide on the Electrocatalytic Activity of PbO2-WC Composite Inert Anodes during Zinc Electrowinning. *J. Electrochem. Soc.* **2017**, *164*, H1064−H1071.
(59) Hiesgen, R.; Morawietz, T.; Handl, M.; Corasaniti, M.; Friedrich, K. A. Insight into the Structure and Nanoscale Conductivity of Fluorinated Ionomer Membranes. *J. Electrochem. Soc.* **2014**, *161*, F1214−F1223.
(60) Cho, M. K.; Park, H.-Y.; Lee, H. J.; Kim, H.-J.; Lim, A.; Henkensmeier, D.; Yoo, S. J.; Kim, J. Y.; Lee, S. Y.; Park, H. S.; Jang, J. H. Alkaline anion exchange membrane water electrolysis: Effects of electrolyte feed method and electrode binder content. *J. Power Sources* **2018**, *382*, 22−29.

DOI: 10.1021/acscatal.8b02217
ACS Catal. 2018, 8, 11688−11698